End-on x-ray backlighting experiments for axial diagnostics of wire-array Z-pinch plasma on PPG-1*

Shen Zhao(赵岫)[1,2], Xinlei Zhu(朱鑫磊)[1], Huantong Shi(石桓通)[1], Xiaobing Zou(邹晓兵)[1], and Xinxin Wang(王新新)[1,†]

[1] *Department of Electrical Engineering, Tsinghua University, Beijing* 100084, *China*
[2] *Shenzhen Institutes of Advanced Technology, Chinese Academy of Sciences, Shenzhen* 518055, *China*

(Received 25 August 2016; revised manuscript received 2 October 2016; published online 30 November 2016)

An X-pinch axial backlighting system has been designed to quantitatively measure the density distribution of wire-array Z-pinch plasmas. End-on backlighting experiments were carried out on a 200 kA, 100 ns pulsed-power generator (PPG-1) at the Tsinghua University. Compared with side-on backlighting, end-on measurements provide an axial view of the evolution of Z-pinch plasmas. Early stages of 2-, 4-, and 8-wire Z-pinch plasmas were observed via point-projection backlighting radiography with a relatively high success rate. The density distribution of Z-pinch plasma on the r–θ plane was obtained directly from the images with the help of step wedges, and the inward radial velocity was calculated. The ablation rates obtained by X-pinch backlighting experiments are compared in detail with those calculated by the rocket model and the results show consistency.

Keywords: X-pinches, axial backlighting, wire-array Z-pinches

PACS: 52.58.Lq, 52.59.Qy **DOI:** 10.1088/1674-1056/26/1/015206

1. Introduction

Wire-array Z-pinches are considered to be a possible approach for driving inertial confinement fusion with a strong ability of x-ray emission and a high transformation efficiency from electrical energy to x-ray energy.[1] However, detailed dynamic physical processes of early stages, which are thought to have an effect on the Rayleigh–Taylor instability and the x-ray radiation capacity, are not fully understood yet and are under intensive research. One of the most appropriate methods to investigate these processes is x-ray backlighting using a pulsed x-ray point source with high spatial and temporal resolution.[2]

X-pinch plasma is a simple and affordable way for universities to acquire sub-nanosecond soft x-ray point sources.[3–7] The side-on backlighting system has been achieved in many universities and national laboratories for the r–z profile measurements of Z-pinch plasmas.[4,5,8–13] Images taken from the r–θ plane are quite necessary for quantitative measurements of the axial distribution of the Z-pinch plasma density. Thus, it is useful to design an axial (end-on) backlighting system. In 2009, an axial backlighting system was constructed on the 1 MA, 100 ns rising time pulsed power generator COBRA in Cornell University.[14] However, the success rate was low due to the high mass X-pinches in their experiments.

In this study, we accomplish the 2-, 4-, and 8-wire Z-pinch experiments on a small current Z-pinch device PPG-1.[13] The success rate of the experiments is increased because relatively lower mass X-pinches can be used as the backlighter. Based on this experimental setup, time resolved backlighting images of 2-, 4-, and 8-wire Z-pinches are obtained. Discussions of several physical parameters such as ablation velocity and ablated mass are then presented. The ablation dynamics of wire array Z-pinches are compared with the rocket model.[15]

2. Experimental setup and diagnostic instruments

The preliminary experimental setup of the axial backlighting system is presented in Fig. 1(a). Different from the side-on backlighting system,[5,16,17] the vertically mounted X-pinch at the side of the Z-pinch array is moved to the bottom and is mounted horizontally. The x-ray film and the step wedge are shifted to the top and laid out horizontally. The anode and the intermediate electrode are shaped as a ring to provide a path for backlighting the x-ray after it penetrates the Z-pinch plasma. The backlighting X-pinch is made of two Mo wires (13–50 μm). For thinner wires such as 13 μm wires, a shunting Cu wire is mounted in parallel with the X-pinch to prevent a secondary x-ray emission from the X-pinch.[10]

In Fig. 1(a), the negative output current of PPG-1 flows through the cathode, the X-pinch wires, the intermediate electrode, the Z-pinch, the anode, the current return rod, and the current return plate successively. The longer current path results in a considerably increased load inductance, and fur-

*Project supported by the National Natural Science Foundation of China (Grant Nos. 11177086 and 51177086), Guangdong Innovative Research Team Program of China (Grant No. 2011S013), the National Key Research and Develop Program of China (Grant No. 2016YFC0105102), the National Basic Research Program of China (Grant Nos. 2012AA02A604 and 2015AA043203), and Beijing Center for Mathematics and Information Interdisciplinary Sciences, China.

†Corresponding author. E-mail: wangxx@tsinghua.edu.cn

© 2017 Chinese Physical Society and IOP Publishing Ltd

ther, a voltage rise of the load section. This leads to vacuum flashover on the surface of the isolation rods, or even vacuum breakdown at the space near the cathode.[16] The breakdown channels cause a decrease of current in the Z-pinch load. In the circumstances where the total output current is high enough,[14] this may not seem to be a serious problem. But unfortunately, there exists a conflict between the X-pinch current and the Z-pinch current. On one hand, a relatively large current is needed for the Z-pinch process to occur evidently; on the other hand, however, the X-pinch current should be reduced to guarantee a high success rate. Reducing the X-pinch current is relatively easy in our work, while a careful redesign of the load section is needed to guarantee a suitable current of the Z-pinch arrays under this circumstance.

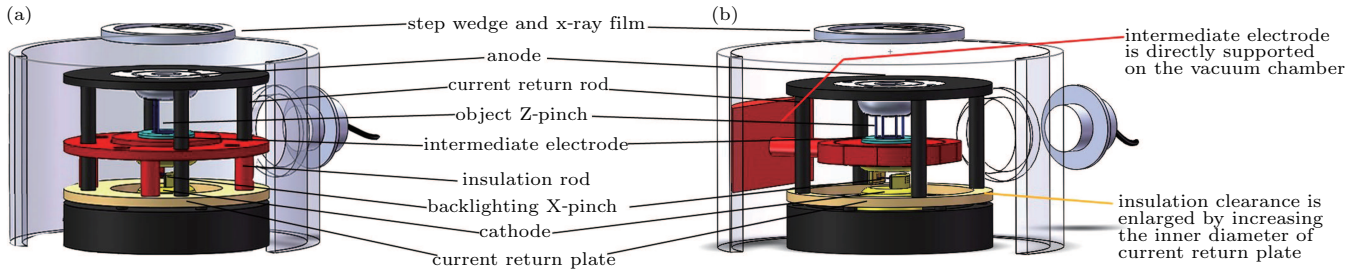


Fig. 1. (color online) Preliminary experimental arrangement for axial backlighting system: (a) the originally designed system, (b) the redesigned system for an adequate Z-pinch current. The vacuum chambers in panels (a) and (b) are of the same size, it is drawn larger in panel (b) for clarification.

The redesign has been performed from two aspects: one is to minimize the load inductance; the other is to reinforce the insulation. To minimize the inductance, the length of the X-pinch is reduced from 14 mm to 6 mm, while that of the Z-pinch is reduced from 2 cm to 1 cm. Moreover, insulation clearance is enlarged by increasing the inner diameter of the current return plate (the light yellow ring in Fig. 1(b)). The insulation rod in Fig. 1(a) is also removed and the intermediate electrode is supported by an arc resistant epoxy resin stand placed on the inner surface of the vacuum chamber, as shown in Fig. 1(b). The overall effect of the redesign is that the current flowing through the Z-pinch can be up to 200 kA. In this experimental setup, about 80% of the Mo X-pinches form a single x-ray source, which means that the success rate is $\sim 80\%$. Meanwhile, the Z-pinch current supply is adequate. Compared with the $\sim 50\%$ success rate in Ref. [14], this is an important improvement of the new backlighting system.

However, 2-wire Z-pinches can emit x-ray under this ~ 200 kA current, which can ruin the experimental results recorded on the film. To avoid this, a shunting Cu wire in parallel with the Z-pinch is used in this specific case to reduce the Z-pinch current to ~ 100 kA. The currents flowing through 2-, 4-, and 8-wire Z-pinches are shown in Fig. 2. The pinching time is 87 ns, as shown in the photoconducting detector (PCD) signal in Fig. 2.

In order to minimize the error arisen from the radial spread of x-ray, the distance from the X-pinch to the object Z-pinch is increased to ~ 80 mm. The distance from the X-pinch to the x-ray film is ~ 650 mm, which gives a magnification of 8.13.

Rogowski coils are used to measure the current waveforms in the X-pinch and the object Z-pinch, whereas PCDs are used to monitor the radiation timing of the X-pinch. The areal density distribution of the Z-pinch plasma is calculated by means of step wedges,[17,18] and the Mo plasma calibrating scale of this method is extrapolated to 16.3 μg/cm^2–2 mg/cm^2, as shown in Fig. 3.

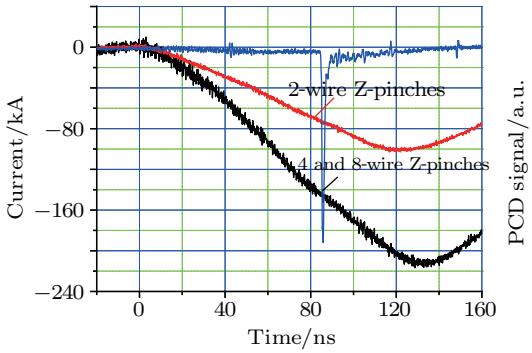


Fig. 2. (color online) Currents flowing through Z-pinches consisted of different wire numbers.

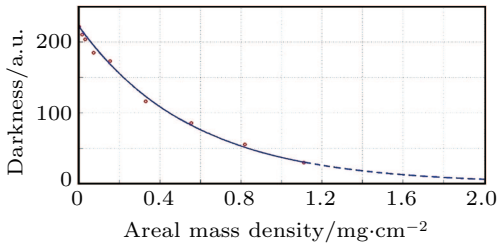


Fig. 3. (color online) Fitted curve between grayscale and areal mass density. (a) $t = 30$ ns, (b) $t = 47$ ns, (c) $t = 60$ ns, (d) $t = 77$ ns, (e) $t = 90$ ns, (f) $t = 108$ ns.

3. Results and discussion

3.1. Experimental results

In our previous experiments, quantitative data on X-pinch timing have been attained and fitted linearly.[19] Thus, backlighting time can be adjusted by changing the linear mass of the X-pinch. In the series of radiographs of a 2-wire Z-pinch in Fig. 4, the backlighting time is respectively 30 ns, 47 ns, 60 ns,

77 ns, 90 ns, and 108 ns. The diameter of the 2-wire Z-pinch is 3 mm, while the initial diameter of the Z-pinch wires is 30 μm. The wire core is defined as the regions where their grayscale is darker than 15% of the darkest region. The wire core diameter is averaged in several directions in our observation.

The wire cores expand to ∼ 330 μm and ∼ 390 μm in Figs. 4(a) and 4(b), respectively. The coronal plasma in Fig. 4(b) seems to be azimuthally symmetric because at this time the global magnetic field is not strong enough. However, as the current continues to rise, the global magnetic field increases and the inward expansion velocity begins to be higher than that in the other directions in Fig. 4(c). The inward streaming coronal plasma reaches the Z-pinch axis and forms a precursor at ∼ 77 ns, which is shown in Fig. 4(d). More plasma is gradually swept to the array axis in Figs. 4(e) and 4(f). Considering the dwell time, the ablation velocity is calculated by following the plasma with a certain density of 0.5 mg/cm^3. For the 2-wire Z-pinch, obvious ablation streams can be seen in Fig. 4(c), and the 0.5 mg/cm^3-plasma is about ∼ 0.42 mm away from the edge, while this density has reached the center in Fig. 4(d). Thus, the ablation velocity should be $(1.5-0.42)$ mm/$(77-60)$ ns $= 6.35$ cm/μs.

Figure 5 shows the three-dimensional (3D) false color images of the plasma density at different time instants calculated using the images in Fig. 4. It is seen that the density of the wire core continues decreasing from ∼ 2 mg/cm^3 (Fig. 5(a)), to 1.6–1.8 mg/cm^3 (Fig. 5(b)), and then to 1.4–1.6 mg/cm^3 (Fig. 5(c)). At the same time, the density of the coronal plasma keeps increasing from less than ∼ 0.1 mg/cm^3 (Fig. 5(a)) to 0.4–0.6 mg/cm^3 (Fig. 5(c)). A clear ablation stream towards the center of the wire array can be seen in Fig. 5(c). Finally, in Figs. 5(e) and 5(f), the boundary between the wire core and the plasma stream becomes blurred. The areal density of the precursor reaches as high as 0.8–1 mg/cm^3 in some particular regions in Fig. 5(f).

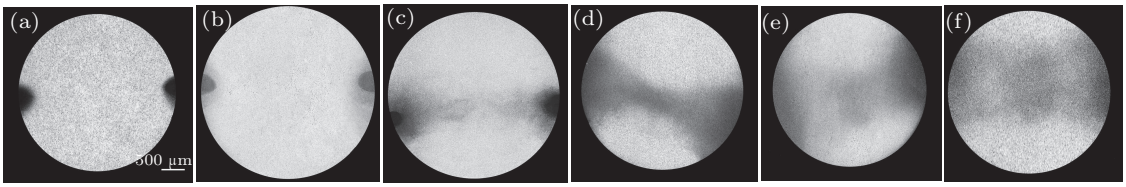


Fig. 4. Time resolved backlighting images of 2-wire Z-pinches: (a) $t = 30$ ns, (b) $t = 47$ ns, (c) $t = 60$ ns, (d) $t = 77$ ns, (e) $t = 90$ ns, (f) $t = 108$ ns.

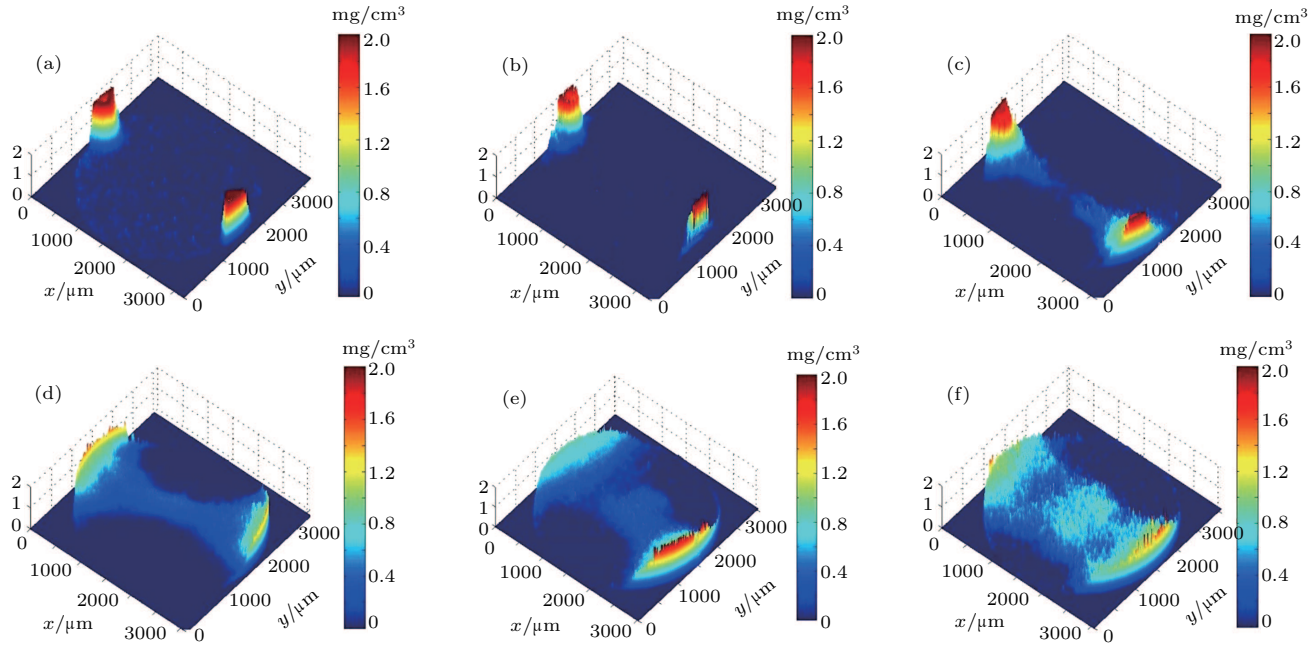


Fig. 5. (color online) 3D false color images showing the plasma density of double wire Z-pinches: (a) $t = 30$ ns, (b) $t = 47$ ns, (c) $t = 60$ ns, (d) $t = 77$ ns, (e) $t = 90$ ns, (f) $t = 108$ ns.

It should be mentioned that although the X-pinches and Z-pinches used are not the same throughout our experiments, the current flowing through them is kept the same. This is because the impedance of the X-pinch and Z-pinch accounts for only a small fraction of the total impedance of the circuit,[19] thus a change in the X-pinch and (or) Z-pinch impedance does not affect the total impedance significantly, resulting in an almost unchanged output current. In other words, the currents in our 2-wire Z-pinch experiments are all very close to (±5 kA) the red waveform in Fig. 2, while the currents in our 4- or

8-wire Z-pinches are all very close to the black waveform in Fig. 2.

It should also be noticed that x-ray emission intensities from the X-pinches are not the same in different experiments. This causes a difference in background exposure level from one film to another. However, the grayscale of the step wedge differs synchronously in different films as the background exposure does. Thus, every film has its specific grayscale-areal mass density curve, although the absolute grayscale value may be different. The calculation of the plasma density of every film is based on its own curve, depending on the relative grayscale of each pixel compared with the background grayscale of the certificate film. Thus, the difference of the background exposure from film to film does not cause a significant error in the plasma density calculation as long as the film is in the linear zone of its characteristic curve. It can be seen from Fig. 5 that the background in all the figures has a zero plasma density.

For 4- and 8-wire Z-pinches, the same experimental procedures were carried out. In these experiments, the current in the Z-pinches was ~ 200 kA. The diameter of the Z-pinch load was enlarged to 4 mm for convenience of wire array assembly.

Time resolved 3D false color images of the plasma density of the 4-wire Z-pinches are shown in Fig. 6. In general, the plasma processes of wire array Z-pinches with different wire numbers are the same. This can be attributed to the fact that in the early stages of Z-pinches, the direction of the magnetic forces caused by the global magnetic field remains towards the center of the wire array, as it is in the 2-wire Z-pinches.

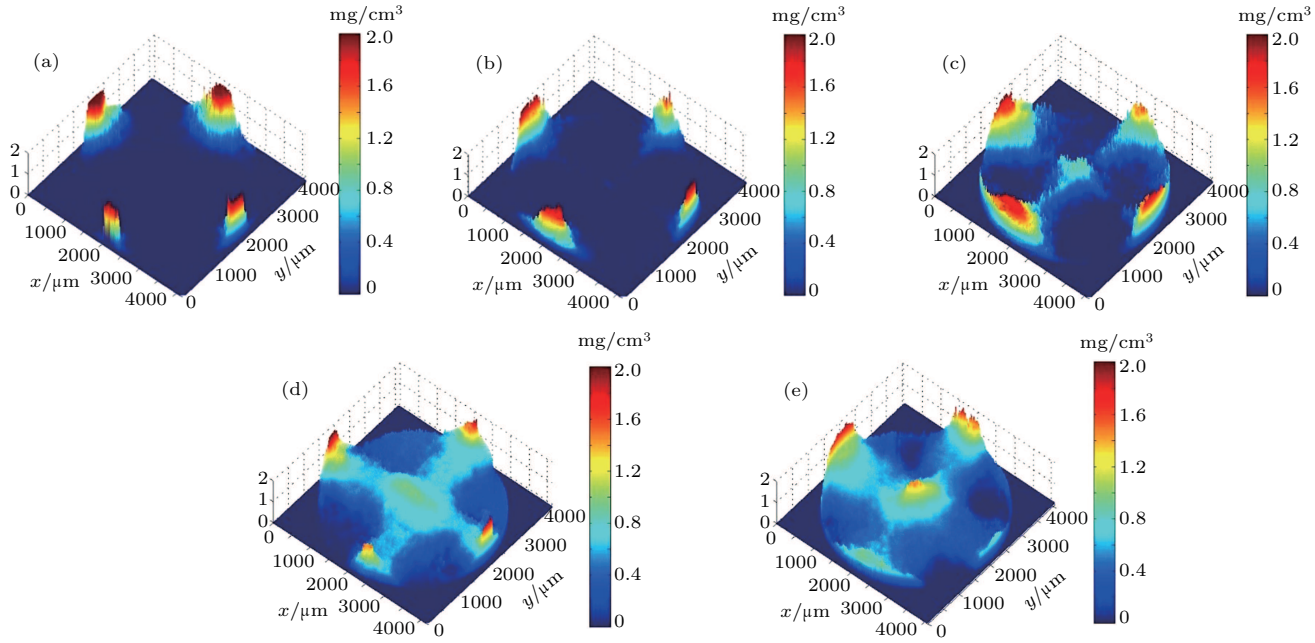


Fig. 6. (color online) 3D false color images showing the areal plasma density of 4-wire Z-pinches: (a) $t = 50$ ns, (b) $t = 71$ ns, (c) $t = 87$ ns, (d) $t = 103$ ns, (e) $t = 147$ ns.

In Fig. 6(a), the diameters of the wire cores in the 4-wire array are about ~ 390 μm at 50 ns, similar to the wire core diameters in the 2-wire Z-pinch at 47 ns. This may be because the current is the same as that in our 2-wire Z-pinch, and that the wires expand individually in the first ~ 50 ns. In Fig. 6(b), the ablation stream is clearly established, and in Fig. 6(c), the stream has reached the center. Thus, the ablation velocity is calculated to be 8.28 cm/μs. A thin precursor plasma (0.1 mg/cm^3) starts to form at the center of the wire array at ~ 71 ns (Fig. 6(b)), while it accumulates to a higher density (0.4–0.8 mg/cm^3 at ~ 87 ns, 0.8–1 mg/cm^3 at ~ 103 ns), as shown respectively in Figs. 6(c) and 6(d). In Fig. 6(e), the maximum density of the precursor can be as high as ~ 1.3 mg/cm^3, comparable with the density of the wire cores.

For Z-pinches consisting of 8×30 μm Mo wires, less (if any) precursor plasma was found beyond the detection threshold even if the backlight timing is ~ 110 ns. 8×30 μm Cu Z-pinch was tested with a peak current of ~ 200 kA for a clearer view of the plasma processes of the 8-wire Z-pinches. Figure 7 shows the time resolved backlighting images and 3D false color images of the 8-Cu-wire Z-pinches.

It is found that even the 8-wire Z-pinch is made of Cu, it takes longer for the precursor to generate. At time less than 78 ns (Fig. 7(b)), hardly any inward ablation stream can be detected on the film. Even at 111 ns, only very thin plasma (less than 0.4 mg/cm^3) appears in the streamers. In order to have a rough estimation of the velocity, we notice that no ablation stream exists at 78 ns, while the ablation stream has reached the array axis at 111 ns. Thus, the ablation velocity is $0.2\ \text{cm}/(111-78)\ \text{ns} = 6.06$ cm/μs.

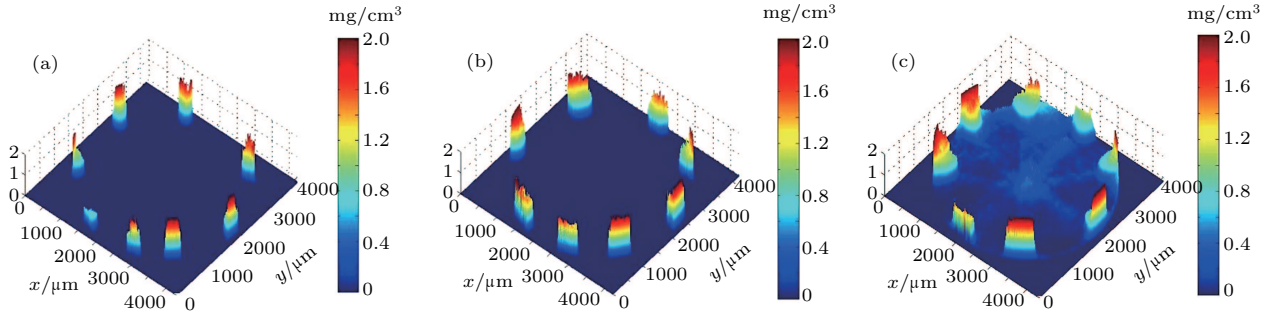


Fig. 7. (color online) 3D false color images showing the plasma density of 8-wire Z-pinches: (a) $t = 37$ ns, (b) $t = 78$ ns, (c) $t = 111$ ns.

3.2. Discussion

It is estimated that the average inward radial velocities of the coronal plasma are 6.35 cm/μs, 8.28 cm/μs, and 6.06 cm/μs for 2-, 4-, and 8-wire Z-pinches, respectively. This is in agreement with the results gained by means of end-on laser probing in the case with approximate current per wire.[15,20–22] It is also found that the ablation velocities are close to each other (in the same order of magnitude), which coincides with the result in the previous work.[23] The ablation velocity of the 4-wire Z-pinches can be slightly higher. This may be due to the fact that the global magnetic field of the 4-wire Z-pinches is larger. The global magnetic field in the Z-pinch arrays can be deduced with the help of Fig. 8. When the wire array is composed of n wires (n is an even number), the global magnetic field experienced by the coronal plasma around one wire is

$$B = \frac{(n-1)\times\mu_0 I_0}{2n\pi D}, \tag{1}$$

where D is the Z-pinch diameter, μ_0 is the vacuum permeability, I_0 is the total driving current of the Z-pinch, n is the wire number in the array, and r is the wire diameter. According to formula (1), when comparing the 4-wire Z-pinches with the 2-wire Z-pinches, B is stronger in the 4-wire Z-pinches (9/4 times) because of larger I_0 and n, and J (current density in each wire) is identical in the 2- and 4-wire Z-pinches (note that I_0 is ~ 200 kA in the 4-wire Z-pinches and ~ 100 kA in the 2-wire Z-pinches). Thus, a stronger $J \times B$ force is generated in the 4-wire Z-pinches, resulting in a faster inward velocity. When comparing the 4-wire Z-pinches with the 8-wire Z-pinches, B is slightly stronger in the 8-wire Z-pinches (7/6 times), while J is only 1/2 of that in the 4-wire Z-pinches, thus the inward velocity is lower.

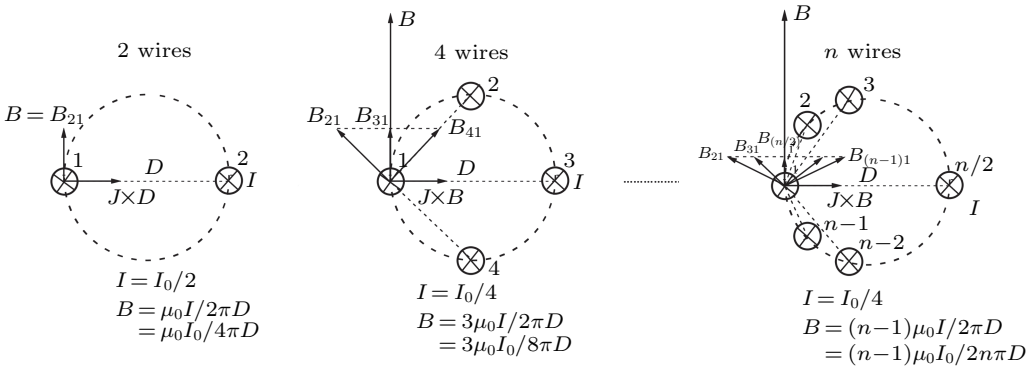


Fig. 8. Schematic of the global magnetic field in Z-pinches of different wire numbers.

Previous studies indicate that the ablated mass $m(t)$ in a wire array Z-pinch can be described by the rocket model[15,24]

$$m(t) = \frac{\mu_0}{4\pi V R_0}\int_0^t I^2(t)\mathrm{d}t, \tag{2}$$

where μ_0 is the vacuum permeability, I represents the current in each wire, V is the ablation velocity of the plasma stream, and R_0 is the radius of the wire core. The mass accumulated in the precursor column of radius R_p (referred to as $m_\mathrm{p}(t)$) can also be calculated assuming that the plasma stays in the precursor after it reaches R_p. This could simply be done by changing the upper limit of the integral of formula (2) to $t-(R_0-R_\mathrm{p})/V$.

For our experiments with the 2-wire Z-pinches, $m(t)$ and $m_\mathrm{p}(t)$ are calculated with formula (2) with the measured velocity 6.35 cm/μs, as shown in Fig. 9. The dependence of $m(t)$ and $m_\mathrm{p}(t)$ on time for each tested wire array can be also obtained by integrating the mass density distributions shown in Figs. 5–7. For $m(t)$, the integration is done over an area which

is clearly inside the core-corona structure, while for $m_p(t)$, the integration is done over a small radius (0.25 mm) around the axis of the wire array. The total mass of the 2-wire Z-pinches is 72 μg.

It is seen in our experiments that the ablated mass is less than 1% of the total mass at ∼50 ns, and it reaches the ∼ 6% level at ∼ 110 ns, the end of our measurements. The $m(t)$ curve calculated by the rocket model gives a reasonable agreement with the experimentally measured ablated mass. Only a very small fraction (less than 0.5% till ∼ 110 ns) of the total mass is in the precursor column, both in theoretical and experimental estimates. This fraction is similar to that obtained with a 16-Al-wire array in Ref. [25].

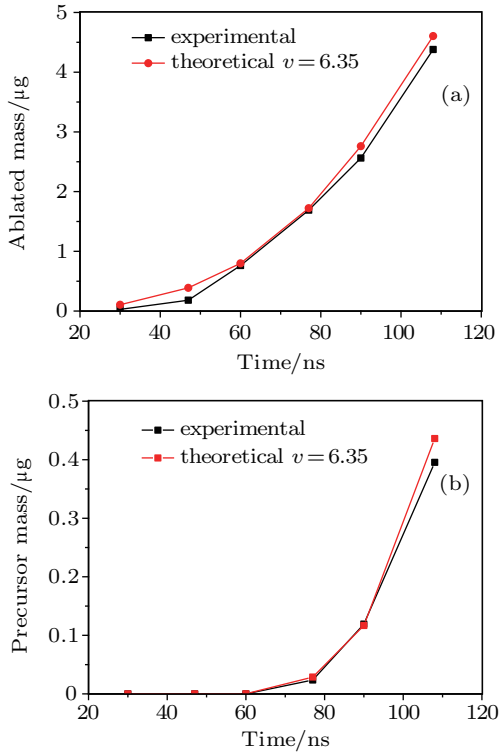


Fig. 9. (color online) Experimentally and rocket model calculated (a) ablated mass and (b) precursor mass as a function of time in 2-wire Z-pinches.

For the 4-wire Z-pinch experiments (total mass 144 μg), $m(t)$ and $m_p(t)$ are calculated by the same method, as shown in Fig. 9. It is seen that the dependence of $m(t)$ and $m_p(t)$ on t calculated using the rocket model coincides with the experimental results in the 4-wire Z-pinches. Both $m(t)$ and $m_p(t)$ are larger in the 4-wire Z-pinches because the total current is twice of that in our 2-wire Z-pinches. A larger current provides a stronger global B field, accelerating more mass to the axis with a higher velocity.

A deviation between the experimental and theoretical values is found in the last data point (t = 147 ns) in Fig. 10. The experimental $m_p(t)$ seems to be smaller than that predicted by the rocket model. The same phenomena are found in Refs. [15] and [25]. This may be because the thermal pressure increases with the density of the precursor, and the plasma would experience a larger force pushing it out of the precursor column. Thus, the accumulation of plasma in the precursor slows down.

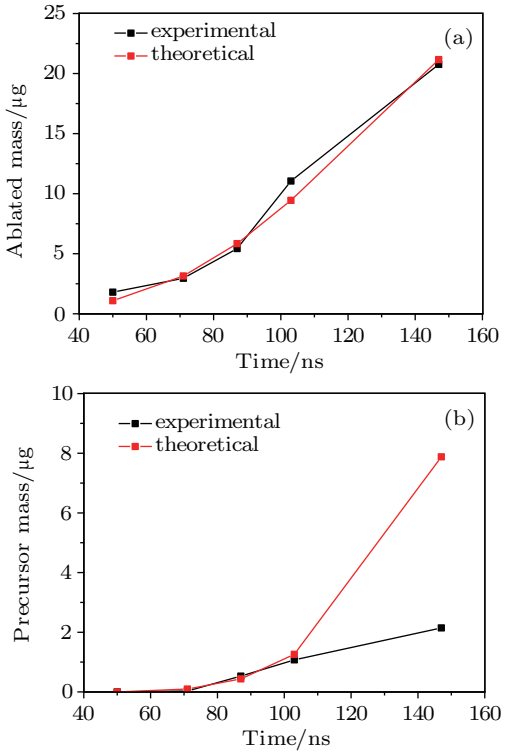


Fig. 10. (color online) Experimentally and rocket model calculated (a) ablated mass and (b) precursor mass as a function of time in 4-wire Z-pinches.

The new studies performed in this work are summarized as follows. 1) The physical parameters are measured by axial X-pinch backlighting, while they were measured by axial laser probing in Refs. [15] and [20]. 2) The line density of the plasma was calculated by integrating the $\langle n_e l \rangle$ distribution in those literatures, while it is directly read out by comparison of the grayscale in this work. This relatively new research method can eliminate the need for an assumption of ion charge, resulting in a more accurate assumption of ablation rate and velocity. Also, the specific data points of the plasma density (Figs. 9 and 10) are not presented in the published literature, probably because the success rate of the backlighting experiments is not high enough. Time resolved evolution of Z-pinch plasma has not been studied quantitatively from the axial field-of-view, especially with low current and less wires. In our work, new data points obtained from X-pinch backlighting are presented and compared with the rocket model, whose reliability has been proved by research on the instability of wire-array Z-pinch plasma.

4. Conclusion

On pulsed power generator PPG-1, an axial backlighting system has been designed and the effect of the increased inductance has been carefully dealt with. Time resolved back-

lighting images of 2-, 4-, and 8-wire array Z-pinches are obtained, which demonstrates the processes of the early Z-pinch stages. Spatial and temporal distribution of Z-pinch plasma density on the r–θ plane is acquired.

The inward ablation velocity and the ablated mass are discussed for Z-pinches with smaller diameter, less wires, and smaller driving current. It is found that the radially inward velocities are in accordance with those in the previous work. The ablated mass density fits well with the analytical rocket model during the early period of ablation, while a deviation is found in the later stage. The ablation velocity estimated by the rocket model is consistent with the experimental measurements. The mass density in the precursor plasma coincides with the rocket model as well.

Acknowledgment

The authors would like to thank Dr. Cheng Ning from the Institute of Applied Physics and Computational Mathematics for helpful discussions on the physics model.

References

[1] Matzen M K, Sweeney M A, Adams R G, Asay J R, Bailey J E and Bennett G R 2005 *Phys. Plasmas* **12** 055503
[2] Volkov G S, Grabovskii E V, Zurin M V, Mitrofanov K N, Oleinik G M and Porofeev I Y 2003 *Instrum. Exp. Tech.* **47** 376
[3] Kalantar D H and Hammer D A 1995 *Rev. Sci. Instrum.* **66** 779
[4] Lebedev S V, Beg F N, Bland S N, Chittenden J P, Dangor A E, Haines M G and Zakaullah M 2001 *Rev. Sci. Instrum.* **72** 671
[5] Zhao T, Zou X B, Wang X X, Zhao Y C, Du Y Q, Zhang R and Liu R 2010 *IEEE Trans. Plasma Sci.* **38** 646
[6] Grabovskii E V, Mitrofanov K N, Oleinik G M and Porofeev I Y 2004 *Plasma Phys. Rep.* **30** 121
[7] Kantsyrev V L, Bauer B S, Shlyaptseva A S, Fedin D A, Hansen S, Presuraa R, Batie S, Cline W, Faretto H, Galloudec B L, *et al.* 2000 *Proc. SPIE* **4144** 51
[8] Liu R, Zou X B, Wang X X, He L Y and Zeng N G 2008 *Laser Part. Beams* **26** 33
[9] Liu R, Wang X X, Zou X B, Zeng N G and He L Y 2008 *Europhys. Lett.* **83** 25002
[10] Liu R, Zou X B, Wang X X, Zeng N G and He L Y 2008 *Laser Part. Beams* **26** 455
[11] Pikuz S A, Shelkovenko T A, Mingaleev A R, Romanova V M, Song B M, Chandler K M, Mitchell M D and Hammer D A 2005 *Proc. SPIE* **5974** 59740L
[12] Pikuz S A, Shelkovenko T A, Sinars D B, Chandler K M and Hammer D A 2001 *Proc. SPIE* **4504** 234
[13] Zou X B, Liu R, Zeng N G, Han M, Yuan J Q, Wang X X and Zhang G X 2006 *Laser Part. Beams* **24** 503
[14] Blesener I C, Greenly J B, Pikuz S A, Shelkovenko T A, Vishniakou S, Hammer D A and Kusse B R 2009 *Rev. Sci. Instrum.* **80** 123505
[15] Lebedev S V, Beg F N, Bland S N, Chittenden J P, Dangor A E, Haines M G, Kwek, K H, Pikuz S A and Shelkovenko T A 2001 *Phys. Plasmas* **8** 3734
[16] Liu R, Wang X X, Zou X B, Zeng N G, He L Y and Liu X 2007 *IEEE Trans. Dielectr. Electr. Insul.* **14** 889
[17] Zhu X L, Zou X B, Zhang R, Luo H Y, Zhao S and Wang X X 2012 *IEEE Trans. Plasma Sci.* **40** 3329
[18] Zhu X L, Zou X B, Zhao S, Shi H T, Zhang R, Luo H Y and Wang X X 2014 *IEEE Trans. Plasma Sci.* **42** 2522
[19] Zhao S, Zhu X L, Zhang R, Luo H Y, Zou X B and Wang X X 2014 *Laser Part. Beams* **32** 437
[20] Lebedev S V, Aliaga-Rossel R, Bland S N, Chittenden J P, Dangor A E, Haines M G and Mitchel I H 1999 *Phys. Plasmas* **6** 2016
[21] Beg F N, Lebedev S V, Bland S, Chittenden N J, Dangor A E and Haines M G 2002 *IEEE Trans. Plasma Sci.* **30** 552
[22] Cuneo M E, Waisman E M, Lebedev S V, *et al.* 2005 *Phys. Rev. E* **71** 046406
[23] Lebedev S V, Ampleford D J, Bland S N, *et al.* 2005 *Plasma Phys. Contr. F* **47** A91
[24] Eduardo M W, Cuneo1M E, Stygar W A, Sasorov P V and Yu E P 2006 *Phys. Plasmas* **13** 062702
[25] Lebedev S V, Beg F N, Bland S N, Chittenden J P, Dangor A E, Haines M G, Pikuz S A and Shelkovenko T A 2001 *Laser Part. Beams* **19** 355